Available online at www.sciencedirect.com
ScienceDirect
Catalysis Today 120 (2007) 276–280
CATALYSIS TODAY
www.elsevier.com/locate/cattod

Hydriding properties of Mg–*x*Ni alloys with different microstructures

Chang Dong Yim [a,*], Bong Sun You [a], Young Sang Na [a], Jong Soo Bae [b]

[a] *Advanced Materials Research Division, Korea Institute of Machinery and Materials, Gyeongnam 641-831, Republic of Korea*
[b] *New Functional Materials Research Division, Korea Institute of Machinery and Materials, Gyeongnam 641-831, Republic of Korea*

Available online 30 October 2006

Abstract

The hydriding properties of Mg–*x*Ni (*x* = 13.5, 23.5 and 33.5 wt%) alloys with different microstructures produced by various processing routes were evaluated in this study. The hydrogen storage capacity and kinetics of hydriding of Mg–*x*Ni alloys were strongly dependent on their microstructures. The capacity and kinetics of hydriding were larger and faster when the average size of the hydriding phase was smaller and the volume fraction of the phase boundary was larger.

Keywords: Microstructure; Catalyst; Hydriding; Dehydriding

1. Introduction

Magnesium has a large potential as a hydrogen storage material due to its low density, abundant resources, low cost, and owing to its superior hydrogen storage capacity compared to other metallic materials. However, the poor kinetic properties for hydriding/dehydriding and its high working temperature have limited the practical application of Mg-based hydrogen storage materials. For this reason, many studies have been sought to improve the hydriding and dehydriding properties of Mg-based materials through several methods, including the addition of alloying elements [1–5], intermetallics [6–8] and oxides [9–11]. In particular, research concerning alloy designs based on the Mg–Ni binary alloy has continued, as it was reported that Ni improves the hydriding/dehydriding kinetics and decreases the working temperature dramatically compared to that of pure Mg in a study by Reilly and Wiswall [12]. Many studies have focused on changes in the hydriding/dehydriding properties of Mg–Ni binary alloys with compositional changes and changes in processing variables [13–16]. Investigations concerning the relationship between the microstructure and the hydriding/dehydriding properties of Mg–Ni binary alloys are, however, rarely carried out although the hydriding/dehydriding properties are strongly dependent on the microstructure. In this study, the microstructural changes in Mg–*x*Ni binary alloys produced by different processing routes are investigated, and the relationship between microstructure and hydriding properties is examined.

2. Experimental

2.1. Preparation of Mg–xNi alloys

A pure Mg (99.9%) ingot was charged into a stainless steel crucible and heated to 1173 K. After the complete melting of the Mg ingot, pure Ni (99.9%) was added to the molten Mg as a chip in order to be quickly solved in order to minimize the evaporation and oxidation of Mg at the high temperature. The amounts of Ni added into the molten Mg were 13.5, 23.5, and 33.5 wt%. Mechanical stirring was carried out in order to homogenize the temperature and composition of the melt and to have the Ni chips solve quickly into the Mg melt. A protective gas mixture of CO_2 and SF_6 gases was blown onto the melt surface in order to prohibit the oxidation and ignition of Mg during heating and melting. The alloy melt was poured into a mold preheated to 473 K after the Ni chips were solved completely into the melt. Gravity casts were cut into appropriate sizes and were inserted in a boron nitride crucible. After the Mg–*x*Ni alloys had melted completely by high frequency induction heating, the melt was injected through a nozzle with a diameter of 2.5 mm onto the surface of a rotating copper wheel at a linear velocity of 35 m/s. The injection

* Corresponding author. Tel.: +82 55 280 3530; fax: +82 55 280 3599.
E-mail address: cdyim03@kmail.kimm.re.kr (C.D. Yim).

0920-5861/$ – see front matter © 2006 Elsevier B.V. All rights reserved.
doi:10.1016/j.cattod.2006.09.020

pressure was 0.5 kg/cm^2 and the distance between the nozzle and the wheel was 1.5 mm. The width and thickness of melt-spun ribbon were 2.5–4 mm and 60–100 μm, respectively. Some parts of the melt-spun ribbon were heat-treated isothermally at 523 K for 1 h in order to produce nanostructured alloys through crystallization of the amorphous phase.

2.2. Observation of microstructure

The specimens for microstructural observation were cut into appropriate sizes from the gravity cast Mg–*x*Ni alloys and were polished mechanically using emery papers and diamond pastes. The microstructures of the gravity cast Mg–*x*Ni alloys were examined using an optical and scanning electron microscopes. Disks with diameters of 3 mm were cut from the melt-spun and heat-treated ribbons and polished using a jet polisher and an ion miller in order to prepare specimens for microstructural observation using a transmission electron microscope. During ion milling, the temperature of the stages was maintained at 173 K using liquid nitrogen in order to prevent an unexpected change of microstructure due to local heating by the electron beam. The phases in Mg–*x*Ni alloys were identified using an XRD and EDS.

2.3. Characterization of hydriding properties

0.5 g powder was pulverized from Mg–*x*Ni alloys produced by different processing routes for a characterization of the hydriding properties. Three hydriding/dehydriding cycles were performed before the measuring of the capacities and kinetics. The capacities and kinetics of hydriding of the samples were measured using Sievert-type equipment. The initial pressure of the hydrogen in reactor was 1.1 MPa and the temperatures of the reactor and channel were 573 and 303 K, respectively. The hydriding time per cycle was 120 min.

3. Results and discussion

Fig. 1 shows the microstructural changes in the gravity cast Mg–*x*Ni alloys with Ni contents. In the hypoeutectic alloy (Fig. 1(a)), the spherical primary solid particles were distributed homogeneously into the fine eutectic matrix. A cellular structure, consisting of fine eutectic phases inside the colonies with different direction, was observed in the near-eutectic alloy (Fig. 1(b)). There were also spherical and polygon crystalline phases which were considered to be solidified by the local segregation of the solute Ni. In the hypereutectic alloy (Fig. 1(c)), the polygon primary solid particles were distributed into the cellular eutectic matrix similar to the near-eutectic alloy.

Fig. 2 shows the results of an XRD analysis carried out to identify the phases solidified in the gravity cast Mg–*x*Ni alloys with Ni contents. There were only two phases, α-Mg (solid solution of Mg and Ni) and Mg_2Ni that solidified from the Mg–*x*Ni alloy melts and the peak intensity of the α-Mg phase decreased while that of the Mg_2Ni phase increased as the Ni content increased.

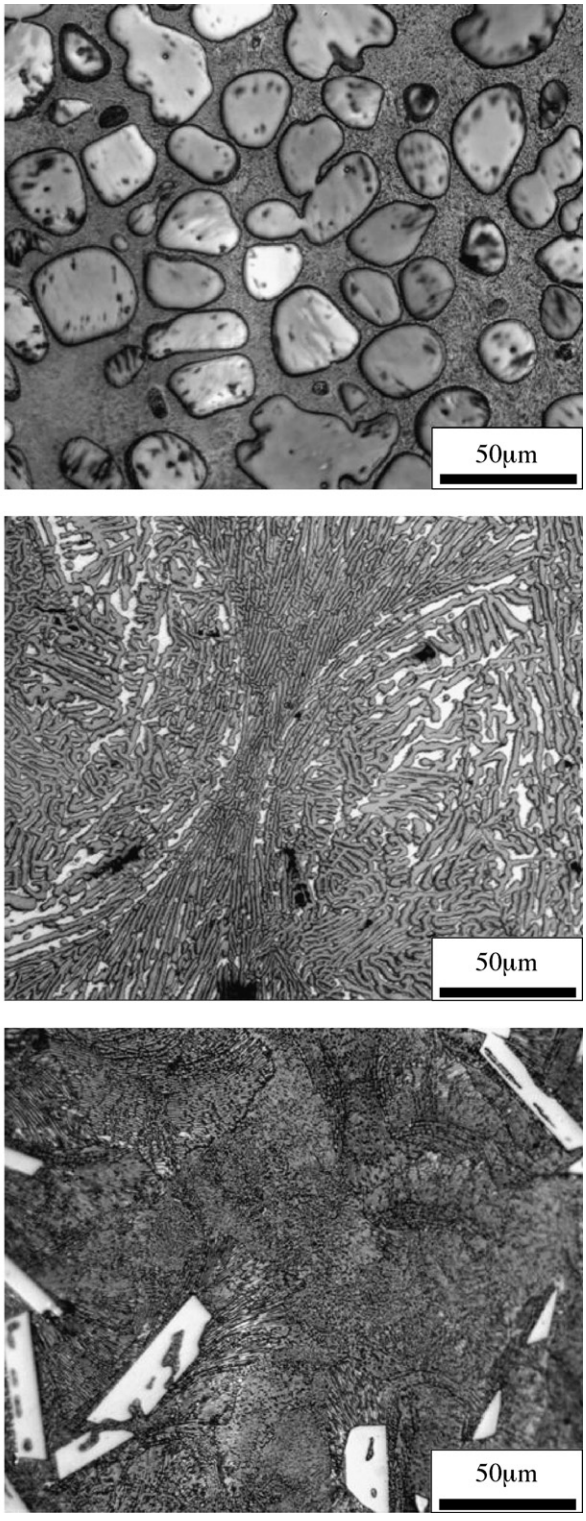

Fig. 1. Microstructures of gravity cast Mg–*x*Ni alloys: (a) $x = 13.5$ wt%; (b) $x = 23.5$ wt%; (c) $x = 33.5$ wt%.

Fig. 3 shows the results of an SEM-EDS analysis carried out in order to identify the phases with different shapes in the gravity cast Mg–23.5 wt% Ni alloys. The spherical crystalline phase was identified as a α-Mg phase in which the solute Ni was solved into Mg, and the polygon crystalline phase was identified as an Mg_2Ni intermetallic compound.

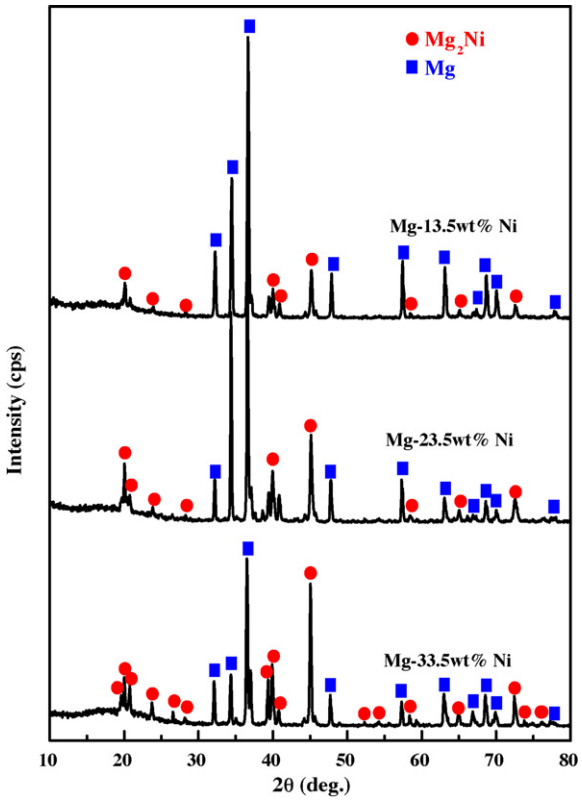

Fig. 2. XRD patterns of gravity cast Mg–*x*Ni alloys.

Fig. 4 shows the hydriding properties of gravity cast Mg–*x*Ni alloys with an Ni content at the third cycle. The capacity of hydrogen absorption was highest in the eutectic alloy. The time for absorption of 90% of the maximum absorption capacity was

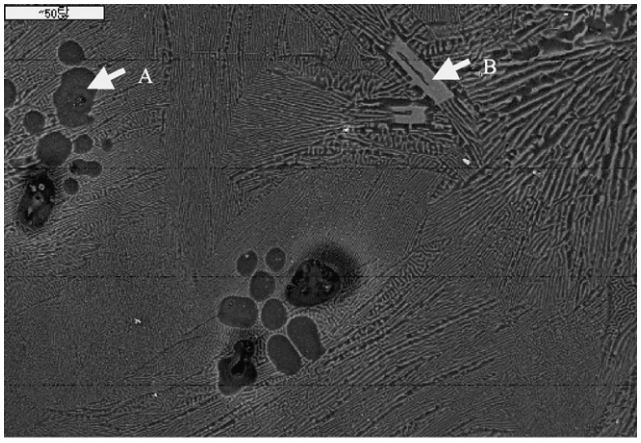

Position	Weight Percent (%)		Atomic Percent (%)	
	Mg	Ni	Mg	Ni
A	99.1	0.9	99.6	0.4
B	44.6	55.4	66.0	34.0

Fig. 3. Results of an EDS analysis of the gravity cast Mg–23.5 wt% Ni alloy.

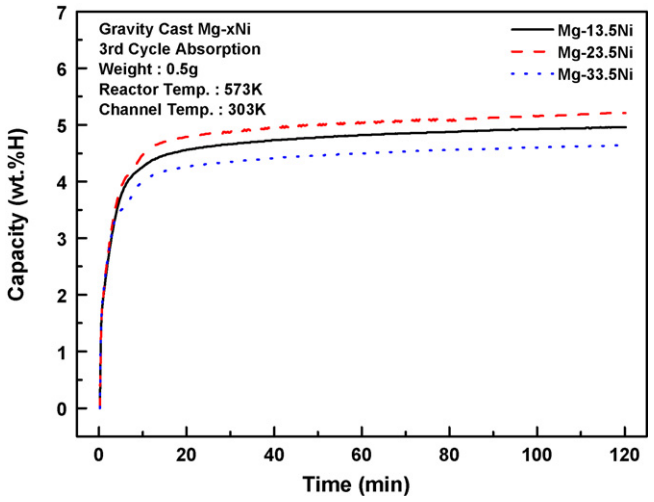

Fig. 4. Hydriding properties of gravity cast Mg–*x*Ni alloys.

similar regardless of the Ni content, which suggests that the hydriding kinetics of the gravity cast Mg–*x*Ni alloys are not strongly dependent on the Ni content. However, the hydriding kinetics of the Mg–*x*Ni alloys are faster than that of pure Mg [17]. The Mg–*x*Ni alloys absorbed 90% of the maximum absorption capacity within 15 min; however, the case of pure Mg required more than 60 min. The hydriding reaction of Mg progresses by a mechanism of nucleation and growth, and the hydriding rate of Mg is controlled by the diffusion of atomic hydrogen [11]. For nucleation of magnesium hydride, hydrogen molecules transported to the surface should be dissociated to hydrogen atoms in order to be diffused into the bulk. Mg_2Ni acts as a catalyst of dissociation of the hydrogen molecule, thus the nucleation of magnesium hydride occurs faster in Mg–*x*Ni alloys than in pure Mg. A small amount of Mg_2Ni (less than 1 wt%) is required as a catalyst for a fast dissociation, which is known as a ''spillover'' mechanism [13]. Hence, the hydriding rate of the Mg–*x*Ni alloys in this study was independent of the Ni content at an early stage due to the fast nucleation. For the growth of the nuclei, the hydrogen chemisorbed on the surface should be transported to the nuclei of the magnesium hydride. The transport of the hydrogen can be carried out through, (1) a diffusion in magnesium hydride, (2) a grain boundary diffusion, (3) a phase boundary diffusion, and (4) a diffusion in the Mg_2Ni phase [14]. Among these routes for hydrogen transport, atomic hydrogen moves fastest along the phase boundary. As shown in Fig. 1, the volume fraction of the phase boundary between the α-Mg and Mg_2Ni phases was highest in the eutectic alloy [15], which resulted in faster growth of magnesium hydride after 5 min.

The microstructural changes and results of the XRD analysis of the melt-spun Mg–*x*Ni alloys with different Ni contents are shown in Figs. 5 and 6, respectively. The nanocrystalline α-Mg phase was distributed into the fine eutectic matrix in the hypoeutectic alloy while only an amorphous phase was observed in the eutectic and hypereutectic alloys, which was similar to the results reported in a previous study [2].

Fig. 7 shows the hydriding properties of melt-spun Mg–*x*Ni alloys with Ni content at the third cycle. The capacities and

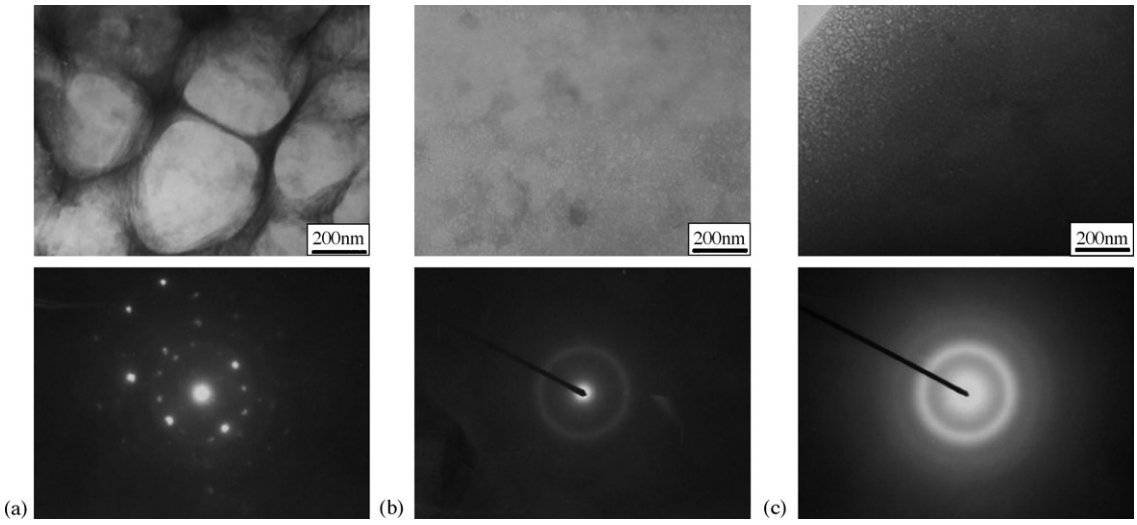

Fig. 5. Microstructures of melt-spun Mg–*x*Ni alloys: (a) x = 13.5 wt%; (b) x = 23.5 wt%; (c) x = 33.5 wt%.

kinetics of hydrogen absorption were highest and fastest in the nanocrystalline hypoeutectic alloy. Vigeholm et al. [16] observed a shrinking core morphology with a continuous phase boundary between α-Mg and MgH_x phases during the formation of magnesium hydride. The nuclei of magnesium hydride grow along the grain boundary and into the α-Mg. After forming a compact hydride layer on the α-Mg surface, the hydriding rate decreases dramatically as the diffusion of hydrogen in the magnesium hydride occurs much more slowly than in the α-Mg [18,19], and the hydriding reaction stops completely when the thickness of the hydride layer exceeds a critical value due to kinetic reasons. Accordingly, the fraction transformed to hydride would be higher in finer grains. As shown in Figs. 4 and 7, the hydriding capacity and kinetic of melt-spun Mg–13.5 wt% Ni alloy consisting of nanocrystalline α-Mg and a fine eutectic matrix were higher and faster than those of the gravity cast Mg–*x*Ni alloys.

Only amorphous phases were observed in the eutectic and hypereutectic alloys, in as the melt-spun state. Although there were only amorphous phases before the hydriding and dehydriding cycles, the amorphous phases were transformed into crystalline phases during first cycle, as the specimens were exposed to a high temperature above the crystallization temperature for an extended time. Further study is needed in order to investigate the relationship between the microstructure and hydriding properties of amorphous alloys.

The microstructure of the Mg–23.5 wt% Ni ribbon heat-treated at 523 K for 1 h consisted of nanocrystalline α-Mg (average size of 150 nm) and an eutectic matrix as shown in Fig. 8. The amorphous phase in the melt-spun ribbon was crystallized into α-Mg and Mg_2Ni phases during the heat treatment.

Fig. 9 shows the hydriding properties of the Mg–*x*Ni alloys with different microstructures. The capacity and kinetic of the alloy with the finer grain structure were higher and faster, respectively. Although the average size of the α-Mg (hydriding phase) was similar to that of the melt-spun Mg–13.5 wt% Ni alloy and heat-treated Mg–23.5 wt% Ni alloy after melt

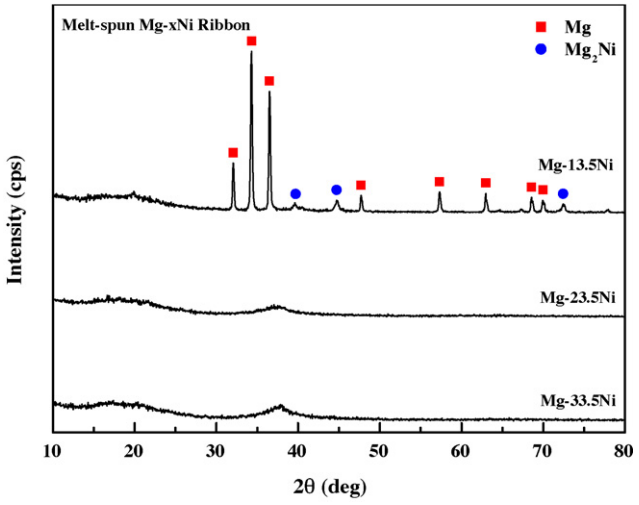

Fig. 6. XRD patterns of melt-spun Mg–*x*Ni alloys.

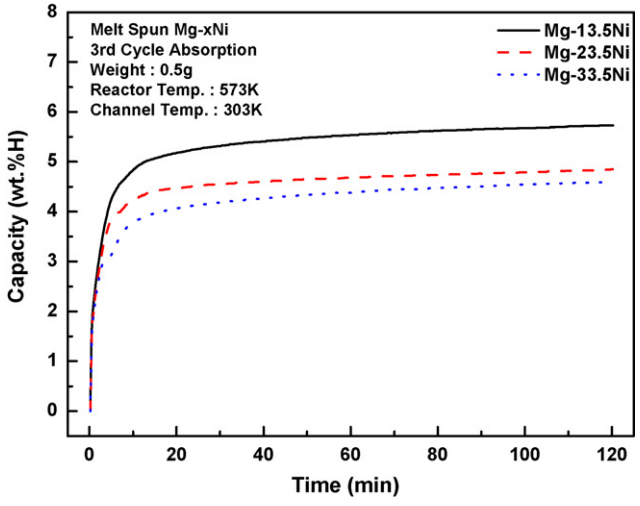

Fig. 7. Hydriding properties of melt-spun Mg–*x*Ni alloys.

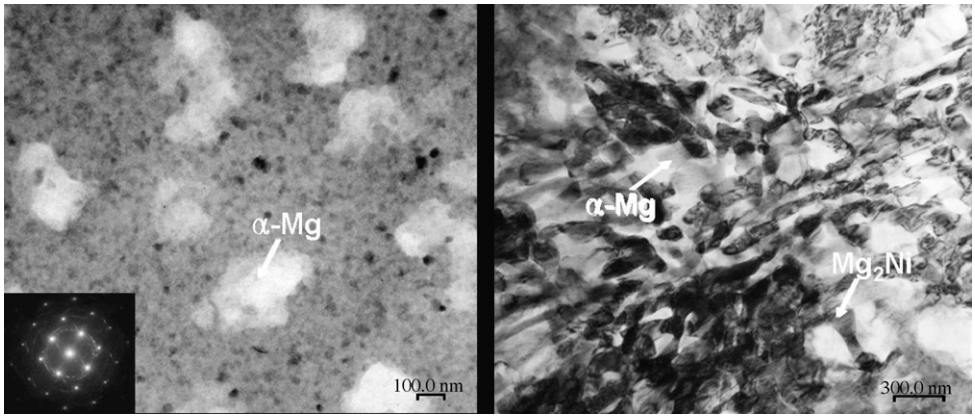

Fig. 8. Microstructure of the Mg–23.5 wt% Ni ribbon heat-treated at 523 K for 1 h.

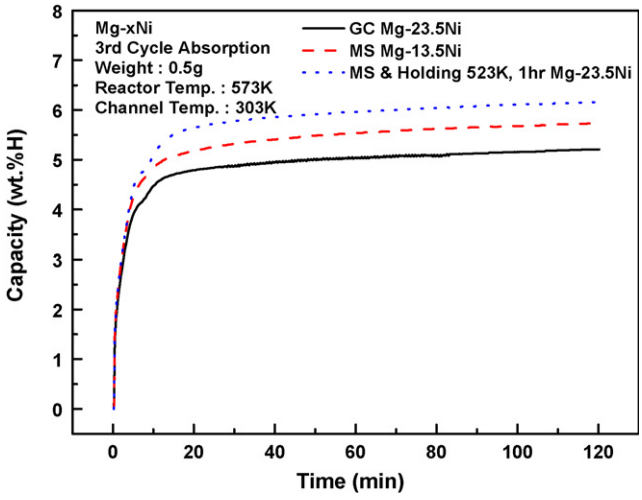

Fig. 9. Hydriding properties of Mg–*x*Ni alloys with different microstructures.

spinning, the capacity and kinetic of the heat-treated Mg–23.5 wt% Ni alloy were higher and faster, respectively, compared to those of as melt-spun Mg–13.5 wt% Ni alloy. It is apparent that this difference results from the difference in the volume fraction of the eutectic matrix. The phase boundaries between the eutectic α-Mg and Mg_2Ni phases acted as a fast diffusion path for atomic hydrogen. The volume fraction of the phase boundary increased as the volume fraction of eutectic matrix increase, which resulted in a higher capacity and kinetic during the hydriding time measured in this study.

4. Conclusions

In this study, the effects of the microstructure on the hydriding properties of Mg–*x*Ni alloys were investigated. α-Mg and Mg_2Ni were major microstructural constituents except in the cases of the melt-spun Mg–23.5 wt% Ni and Mg–33.5 wt% Ni alloys. The Mg_2Ni phase acted as a catalyst of dissociation of the hydrogen molecule, which resulted in a faster nucleation of magnesium hydride compared to pure Mg. It became apparent that the hydriding properties were strongly dependant on the average size of the hydriding phase and volume fraction of the phase boundary. The capacity and kinetic of hydrogen absorption were higher and faster, respectively, when the average size of the hydriding phase was smaller and the volume fraction of the phase boundary was higher.

Acknowledgements

This work was financially supported by the Hydrogen Energy R&D Center, one of the 21st Century Frontier R&D Programs, funded by the Ministry of Science and Technology of Korea.

References

[1] M. Au, J. Wu, Q. Wang, Int. J. Hydrogen Energy 20 (1995) 141.
[2] K. Tanaka, Y. Kanda, M. Furuhashi, K. Saito, K. Kuroda, H. Saka, J. Alloys Comp. 293–295 (1999) 521.
[3] T. Spassov, V. Rangelova, N. Neykov, J. Alloys Comp. 334 (2002) 219.
[4] M. Bououdina, Z.X. Guo, J. Alloys Comp. 336 (2002) 222.
[5] N.E. Tran, M.A. Imam, C.R. Feng, J. Alloys Comp. 359 (2003) 225.
[6] G. Liang, J. Huot, S. Boily, A. Van Neste, R. Schulz, J. Alloys Comp. 297 (2000) 261.
[7] M. Khrussanova, J.-L. Bobet, M. Terzieva, B. Chevalier, D. Radev, P. Peshev, D. Darriet, J. Alloys Comp. 307 (2000) 283.
[8] P. Wang, A.M. Wang, B.Z. Ding, J.Q. Hu, J. Alloys Comp. 334 (2002) 243.
[9] W. Oelerich, T. Klassen, R. Bormann, J. Alloys Comp. 315 (2001) 237.
[10] W. Oelerich, T. Klassen, R. Bormann, J. Alloys Comp. 322 (2001) L5.
[11] M.Y. Song, J.-L. Bobet, B. Darriet, J. Alloys Comp. 340 (2002) 256.
[12] J.J. Reilly, R.H. Wiswall, Inorg. Chem. 7 (1968) 2254.
[13] L. Zaluski, A. Zaluska, P. Tessier, J.O. Ström-Olsen, R. Schulz, J. Alloys Comp. 217 (1995) 295.
[14] G. Liang, S. Boily, J. Huot, A. Van Neste, R. Schulz, J. Alloys Comp. 268 (1998) 302.
[15] C.D. Yim, Y.M. Moon, B.S. You, Y.S. Na, J.S. Bae, Met. Mater. Int. 10 (2004) 605.
[16] B. Vigeholm, J. Koller, B. Larsen, A.S. Pedersen, in: T.N. Veziroglu, J.B. Taylor (Eds.), Hydrogen Energy Progress, vol. V, Pergamon, Oxford, 1984, p. 1455.
[17] A. Zaluska, L. Zaluski, J.O. Ström-Olsen, J. Alloys Comp. 288 (1999) 217.
[18] J. Rydén, B. Hjörvarsson, T. Ericsson, E. Karlsson, A. Krozer, B. Kasemo, Z. Phys. Chem. Neue Folge 164 (1989) 1259.
[19] J. Topler, H. Buchner, H. Saufferer, H. Knorr, W. Prandl, J. Less-Common Met. 88 (1982) 397.